

# Frequency Map Analysis at CesrTA

J. Shanks

## I. FREQUENCY MAP ANALYSIS

### A. Overview

The premise behind Frequency Map Analysis (FMA) is relatively straightforward. By sampling turn-by-turn (TBT) data (typically 2048 turns) across a grid in position-space, one can map the coordinates  $(x, y)$  to a point  $(Q_x, Q_y)$  in frequency-space. This mapping is done by an interpolated FFT on the first 1024 turns of the TBT data. For stable orbits, the tune should be well-established after 1024 turns. One can consider the tune shift between the first and last 1024 turns of TBT data as a comment on the stability of the orbit. If the tune shift is relatively large ( $\sim 0.1$ ), the particle's motion is chaotic and represents an unstable orbit.

The large amount of information from FMA can be analyzed in two ways. First, one can plot the data as a 2D histogram in  $(x, y)$ -space, with a color scale to indicate the magnitude of tune shift between the first and last half of TBT data. This amounts to a dynamic aperture (DA) plot, where the boundary of the stable region indicates an estimate of the dynamic aperture of the machine.

Second, one can use the first half of TBT data for the initial tunes  $(Q_x^{(1)}, Q_y^{(1)})$  and use these values as the axes in frequency-space. The data can then be plotted as a scatter plot, with a color scale indicating the tune shift between the first and second half of TBT data.

Both representations of the FMA are Poincaré surfaces, taken at an arbitrary starting position  $s=0$  in the ring. These two interpretations are equivalent, and one of the primary goals of frequency mapping is to determine how one surface maps onto the other.

When plotting the frequency map and dynamic aperture, we use a “diffusion index”  $D$ , defined as:

$$D = \sqrt{\left(Q_x^{(2)} - Q_x^{(1)}\right)^2 + \left(Q_y^{(2)} - Q_y^{(1)}\right)^2} \quad (1)$$

In other words,  $D$  is the RMS tune shift between the first and second half of the TBT data.

### B. Features in Frequency Space

#### 1. Non-Definite Torsion and Directions of “Fast Escape”

Many of the dominant features in frequency maps result from properties of the torsional matrix  $M$ . Laskar goes through the details in his paper, but we will briefly discuss it here. Define  $M$  as:

$$M \approx \left( \frac{\partial^2 H_0(I)}{\partial I^2} \right) \quad (2)$$

where  $I$  is the amplitude (normalized?), and  $H_0$  is the integrable Hamiltonian. (See Laskar's formalism [1] for further detail)

This  $2 \times 2$  Jacobian matrix is equivalent to a generalization of the amplitude-dependent tune shift (neglecting synchrotron oscillations). If the torsion matrix  $M$  is a matrix describing a definite quadratic form, solutions exist with finite time stability that do not exist if  $M$  describes a non-definite torsion. If the torsion is non-definite, then we will see directions of “fast escape” in our frequency map.

If we let  $M^{-1} = \begin{pmatrix} a & c \\ c & b \end{pmatrix}$  and  $V = (x, y)$ , then the vector  $V$  is an isotropic direction (leading to a direction of fast escape) if  $V^T M^{-1} V = ax^2 + 2cxy + by^2 = 0$ . The punchline is this: if  $\det(M) > 0$ , the quadratic form is definite and no isotropic directions exist— that is, no directions of fast escape exist and the motion remains bounded. If  $\det(M) < 0$ , two isotropic directions emerge which act as asymptotes for frequency diffusion, and fast escape may occur.

## 2. Frequency Map Folding

A fold in the frequency map occurs if  $\det(M)$  changes sign in the region of the tune plane spanned by the frequency map. The fold occurs along the line  $\det(M) = 0$ , and the frequency map will have very different characteristics before and after the fold. Before the fold, the torsion should be positive in order to ensure stability of the beam. After the fold, the torsion will become negative, leading to directions of fast escape. It is important to ensure that under normal operating conditions (tunes and amplitudes), one does not enter any regions where directions of fast escape may exist.

## II. SUMMARY: FMA AT OTHER FACILITIES

Frequency mapping has been performed at many other facilities, as summarized by Nadolski and Laskar in PRST:AB [2]. The frequency maps for every machine will be drastically different, and depend strongly on the sextupole distribution. A small change in sextupole strengths can radically change the map.

In order to gain some sense of scale or perspective, we can consider the footprint of other machines' frequency maps in  $(Q_x, Q_y)$ -space. Footprints can range anywhere from  $[0.06 \times 0.05]$  (SOLEIL, after optimization) to  $[1.2 \times 0.2]$  (ESRF). It is not uncommon to see folds and directions of fast escape in frequency maps that Nadolski and Laskar deem acceptable, as long as they occur outside the normal operating regime.

The authors also note that the dynamic aperture is overestimated by this technique, in the sense that resonance lines will limit the DA at much smaller amplitudes than indicated by the plots. This will be discussed in more detail in a later section.

## III. FMA AT CESRТА: CTA\_ 2085MEV\_ 20090516

For the first part of this study we will focus on the cta\_2085mev\_20090516 "NORM" optics for CesrTA. We will only consider the simplest case of an ideal lattice with a flat orbit for now. In each scenario, coordinate-space is sampled in constant steps of  $80\mu\text{m}$  over a region large enough to span the entire dynamic aperture (typically  $\sim 20\text{mm} \times 20\text{mm}$ ). 2048 turns are tracked. An interpolated FFT with a Hanning window is used to determine the tunes from the first and last 1024 turns. Each FMA job is sliced into roughly 500 parallel jobs, each job consisting of a single y-coordinate and all desired x-coordinates. The resulting outputs are then combined for analysis in a Python script. Additionally, an interactive Python script was used in determining how the FM maps back to coordinate space.

Two sextupole distributions are considered. The first is a simple 2-family (2fam) distribution, only optimized to achieve the desired chromaticities. The second distribution was optimized using Bengtsson's prescription [3] to minimize resonances, amplitude-dependent tune shifts, and maximize dynamic aperture. Tune scans for the two sextupole distributions are shown in figure (1).

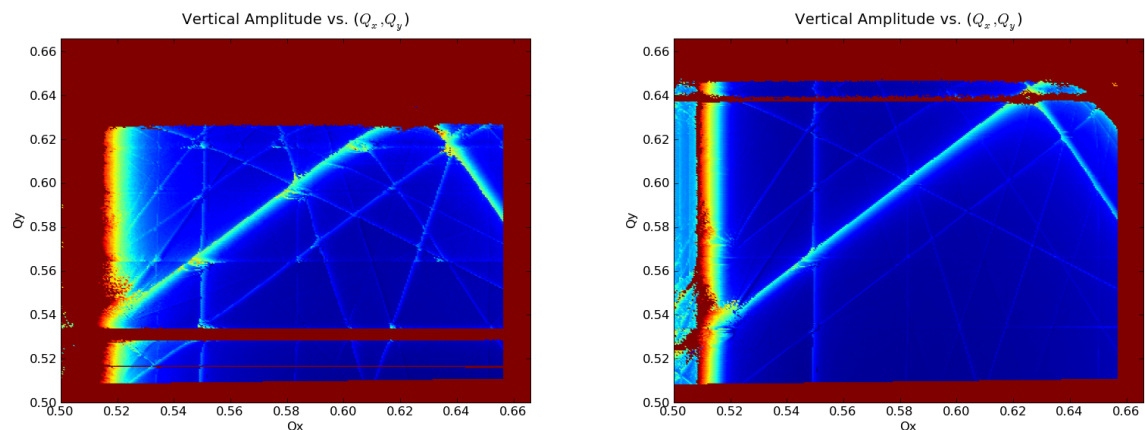


FIG. 1: Tune scans for the two sextupole distributions being analyzed. Left: two-family (2fam). Right: optimized distribution using Bengtsson's formalism.

The design working point for the 2009.05.16 lattice is (0.571, 0.628). This will be taken as the working point for initial analysis.

### A. 2-Family Sextupoles

Figure (2) shows the dynamic aperture and frequency map for the 2-family sextupoles with the original tunes.

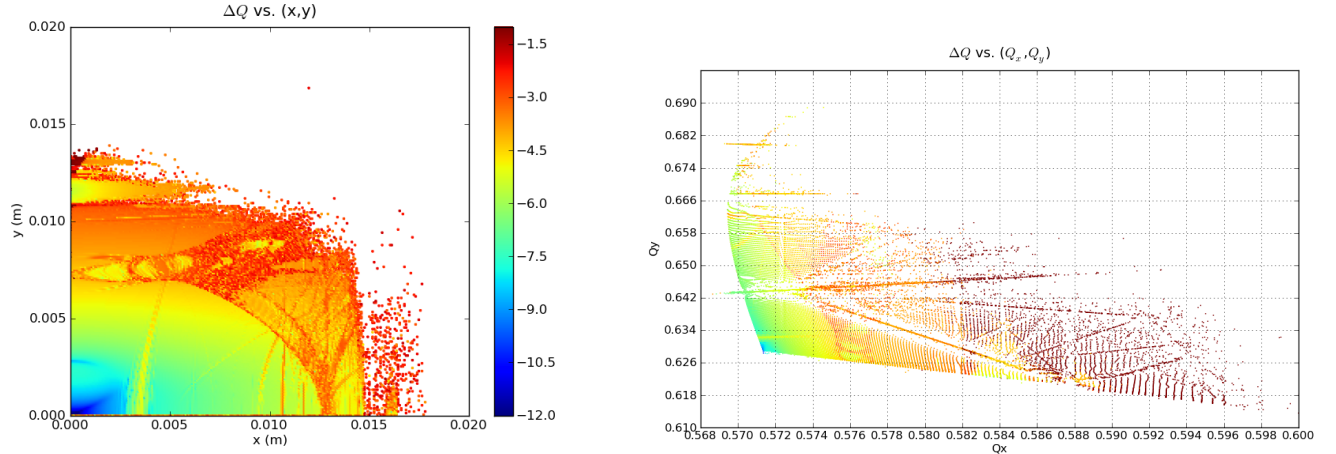


FIG. 2: FMA for 2-family sextupole distribution, original working point of (0.571, 0.628).

The color scales are proportional between the two plots. First, some global remarks about this frequency map. The footprint of this frequency map is roughly  $[0.030 \times 0.088]$ , which is well within the range seen in Nadolski and Laskar's studies. If anything, this footprint is relatively small compared to other unoptimized sextupole distributions. We do not see any folds in this map, but there appear to be paths of fast escape along several resonances. It is interesting to note that starting coordinates near a resonance tend to be either attracted toward or repelled from the resonance. This phenomenon is discussed by Laskar [1].

Next, we can identify what resonances are present in the frequency map and determine how they map back to coordinate-space. See figure (3).

It is interesting to note that the nearest matches for resonances are all offset from the simulated data by the same amount, (0.000879, 0.000946). It is not clear at this time what caused this shift.

The resonances in figure (3) can be mapped back into coordinate space by observing significant features. To help with this process, an interactive Python script was developed. This allows the user to select points in frequency space, and the corresponding location in coordinate space is highlighted. See figure (4).

The node at (0.5875, 0.622) lies along the x-axis far from the working point, and therefore corresponds to the point (13mm, 0mm) in the dynamic aperture plot. The  $3Q_x + 2Q_y = 3$  resonance is therefore the leftmost curve in this junction, branching up and to the left toward (0mm, 8mm). The node at (0.574, 0.644) in the tune plane maps back to (5mm, 7.5mm) in coordinate space. The  $3Q_y = 2$  resonance maps to a horizontal line at roughly  $y = 11mm$ .

It is likely that the dynamic aperture is not nearly as large as this simulation would have one think. The  $3Q_x + 2Q_y = 3$  resonance is likely strong enough to limit the dynamic aperture to approximately  $13mm \times 8mm$ , rather than  $15mm \times 13mm$ .

### B. Optimized Sextupoles

Next, consider the optimized sextupole distribution. DA and FM plots are shown in figure (5).

Again, a few global remarks first. The first immediately apparent feature in the FM is the introduction of a fold along the right edge of the map. Many lines of fast escape are evident after the fold, in the  $\det(M) < 0$  region. The optimized distribution has a footprint of about  $[0.012 \times 0.088]$ . Vertically this is nearly identical to the 2fam distribution, however horizontally this is a factor of three smaller.

Several features can be mapped back to coordinate space. See figure (6). The fold occurs along a line stretching vertically from (11mm, 0mm) to (14mm, 12mm), arcing to the left. This line is not visible in the DA plot. The

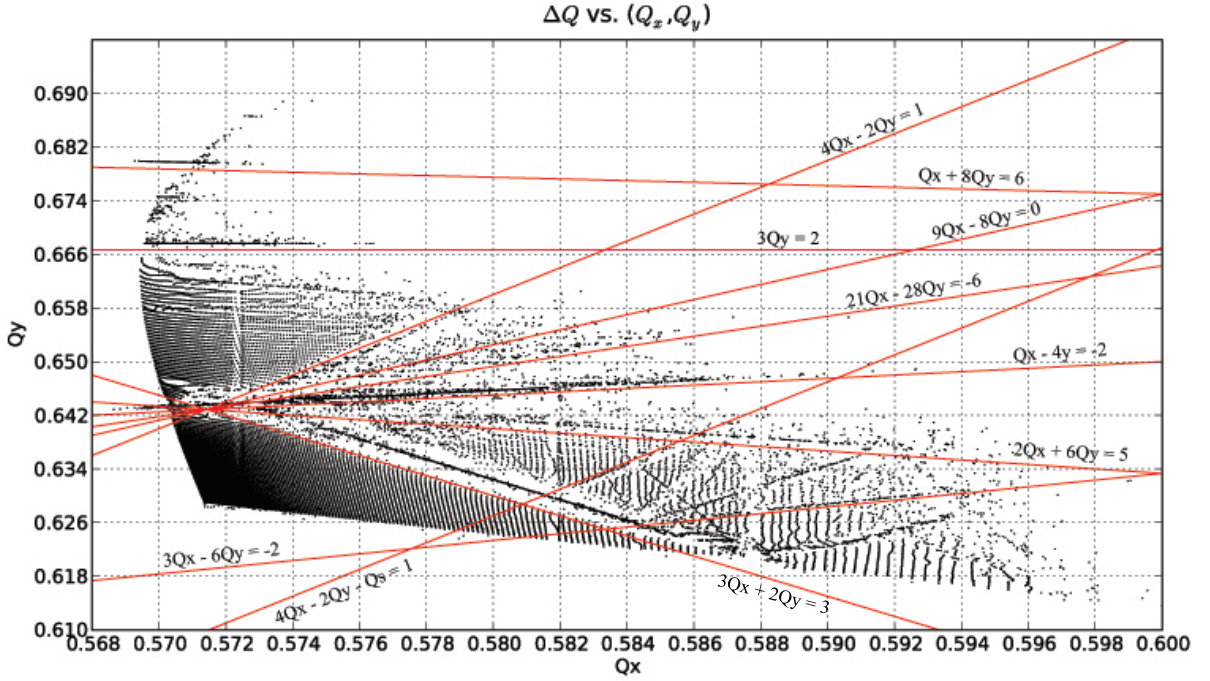


FIG. 3: Labeling the resonances found in the FM from figure (2).

$3Q_y = 2$  resonance line is obvious in the FM, and maps back to a distorted ellipse at  $y = 11mm$  and returning at  $y = 12.5mm$ . The grouping of resonances around  $(0.571, 0.646)$  correspond to several of the same resonances seen in the 2fam frequency map, though again the closest rational resonances are offset from the frequency map by roughly  $+0.001$  in  $Q_x$ .

#### IV. PROPOSED WORKING POINT

To further understand properties of the frequency map, a second working point should be explored. The working point  $(0.578, 0.542)$  looks to be clear of resonances and may be a good choice for a new working point. We now repeat the analysis for this new point. Explicit mapping between DA and FM has not been analyzed yet.

##### A. 2-Family Sextupoles

The dynamic aperture and frequency map for the 2fam sextupole distribution using the new working point is shown in figure (7). The horizontal span in frequency-space has increased from 0.032 to 0.04, but the vertical span has remained roughly the same. Several resonances are now evident that aren't attractors or repellers, and only show up in a color plot.

The effective dynamic aperture has drastically changed from  $[11mm \times 7.5mm]$  to  $[5mm \times 10mm]$ .

##### B. Optimized Sextupoles

The dynamic aperture and frequency map for the optimized sextupole distribution using the new working point is shown in figure (8).

Again, the dynamic aperture has drastically changed from  $[20mm \times 7.5mm]$  to  $[10mm \times 10mm]$ . The original working point has a much larger region with  $D < -6$ , indicating a larger region of stability. However, the situation is reversed when interpreting the frequency map. Although the fold is still present, the new torsion-positive region is larger than for the original working point. By changing the working point we've decreased the DA slightly, while increasing the stable region in the frequency map.

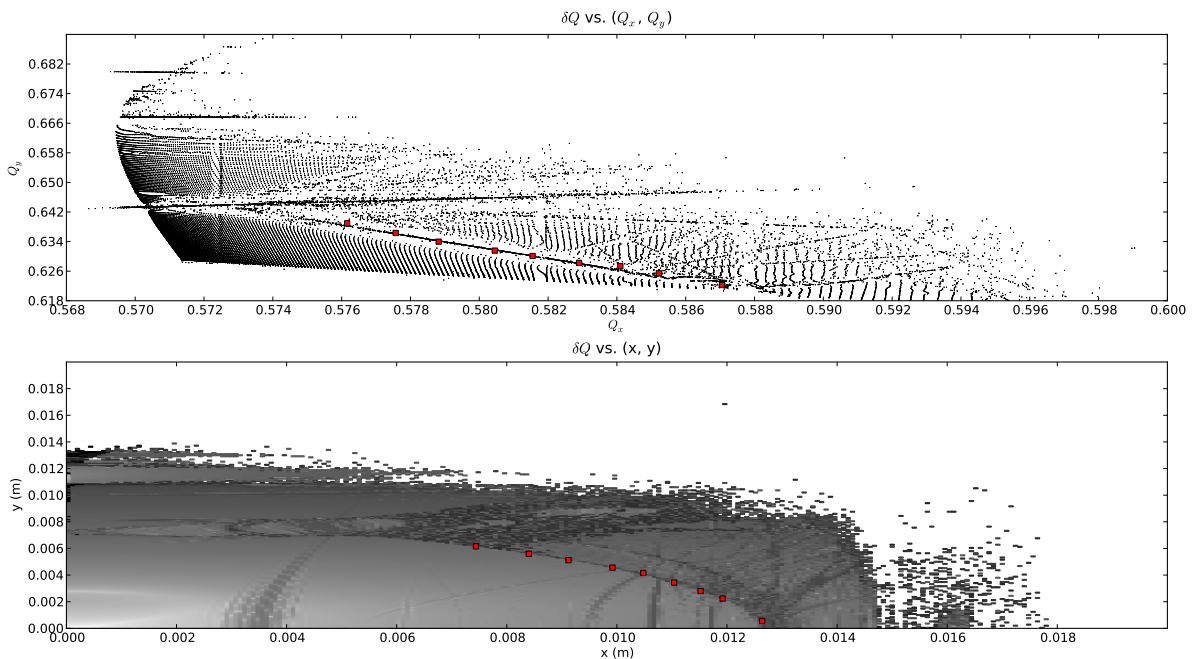


FIG. 4: Interactive Python utility for visualizing how points in frequency space map back to coordinate space. Here, points along the  $3Q_x + 2Q_y = 3$  resonance in the 2fam frequency map are selected, and their corresponding locations in coordinate space are shown.

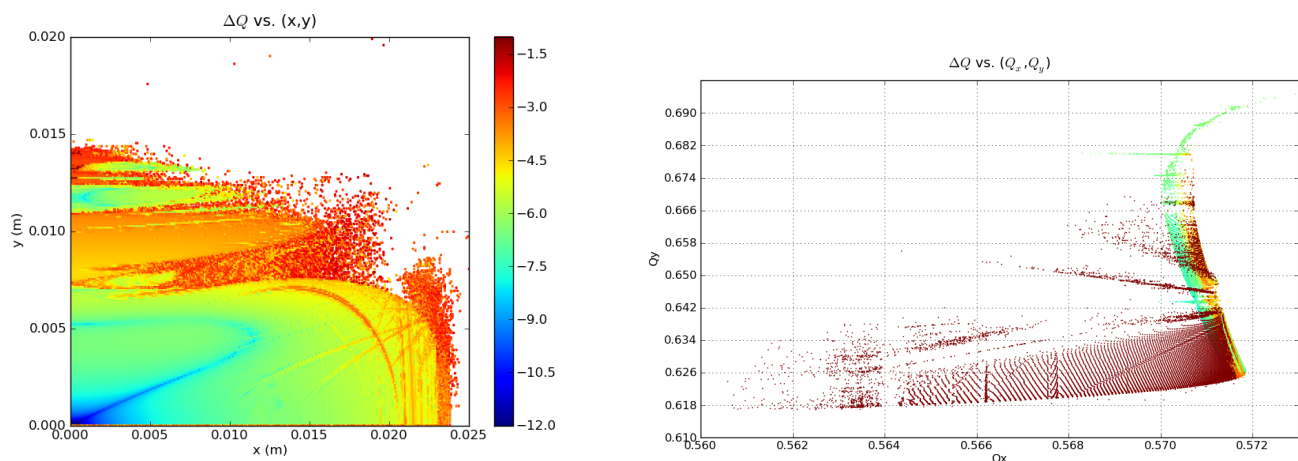


FIG. 5: FMA for optimized sextupole distribution, original working point of  $(0.571, 0.628)$ .

## V. SUMMARY

The techniques and analysis tools have been developed for understanding and interpreting frequency maps. It is now possible to determine what resonances in frequency space are restricting the dynamic aperture in coordinate space. Tolerances for paths of fast escape and folds in frequency space are not yet well understood. Further investigations are required to understand why simulated frequency map data is offset by a constant from theoretical resonance lines.

---

[1] J. Laskar, Frequency Map Analysis and Particle Accelerators, Proceedings of the 2003 Particle Accelerator Conference

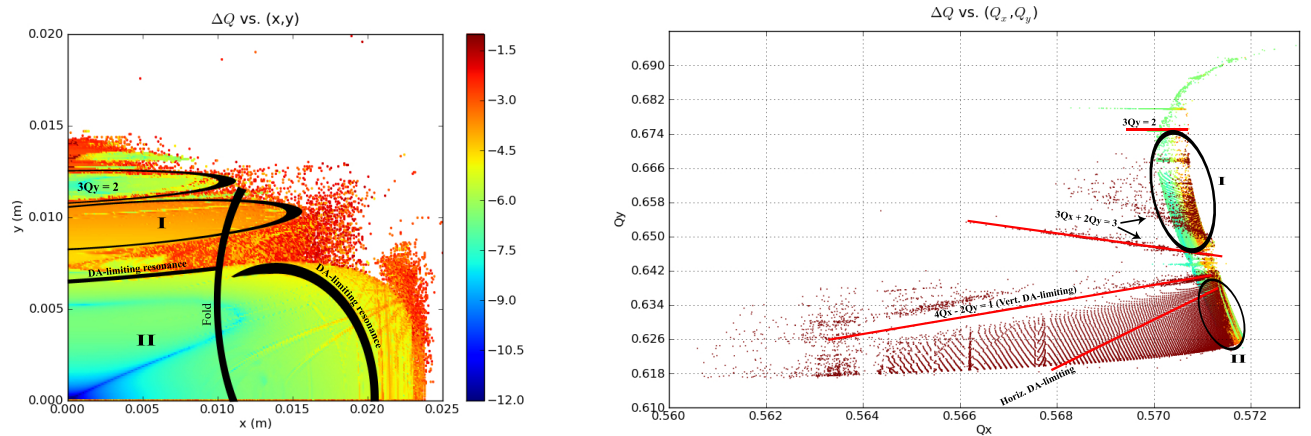


FIG. 6: Labeling the resonances found in the FM from figure (5). The mapping of regions (1) and (2) are shown. The fold is not apparent on the dynamic aperture before labeling. Areas I and II are on the  $\det(M) > 0$  side of the fold, as is the working point.

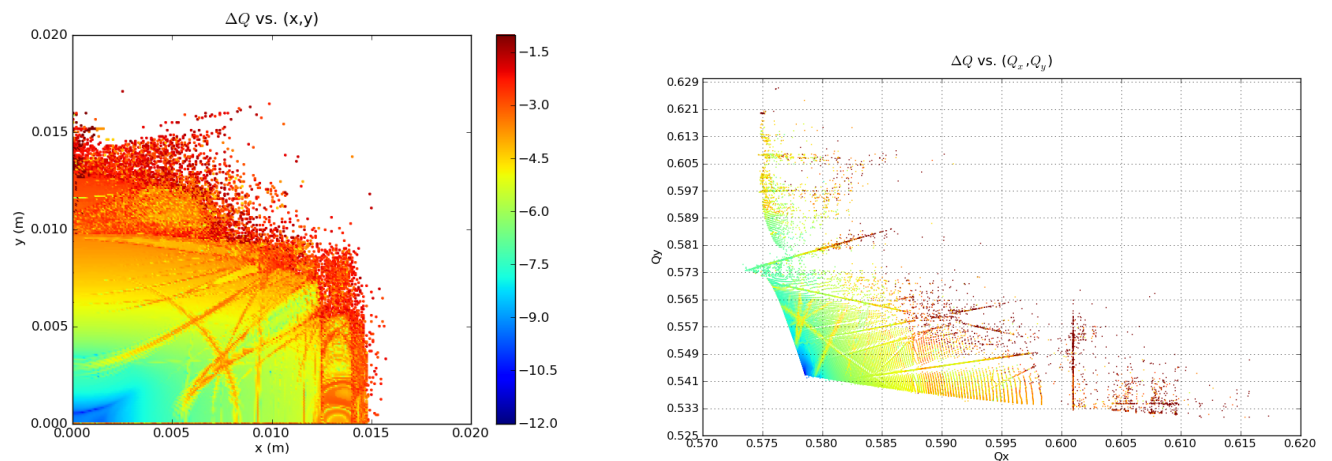


FIG. 7: FMA for 2-family sextupole distribution, with new working point of  $(0.578, 0.542)$ . Vertical grid spacing is identical to figure (2), however the horizontal span is now larger.

- [2] L. Nadolski, J. Laskar, Review of Single Particle Dynamics for Third Generation Light Sources through Frequency Map Analysis
- [3] J. Bengtsson, The Sextupole Scheme for the Swiss Light Source (SLS): An Analytic Approach, SLS Note 9/97

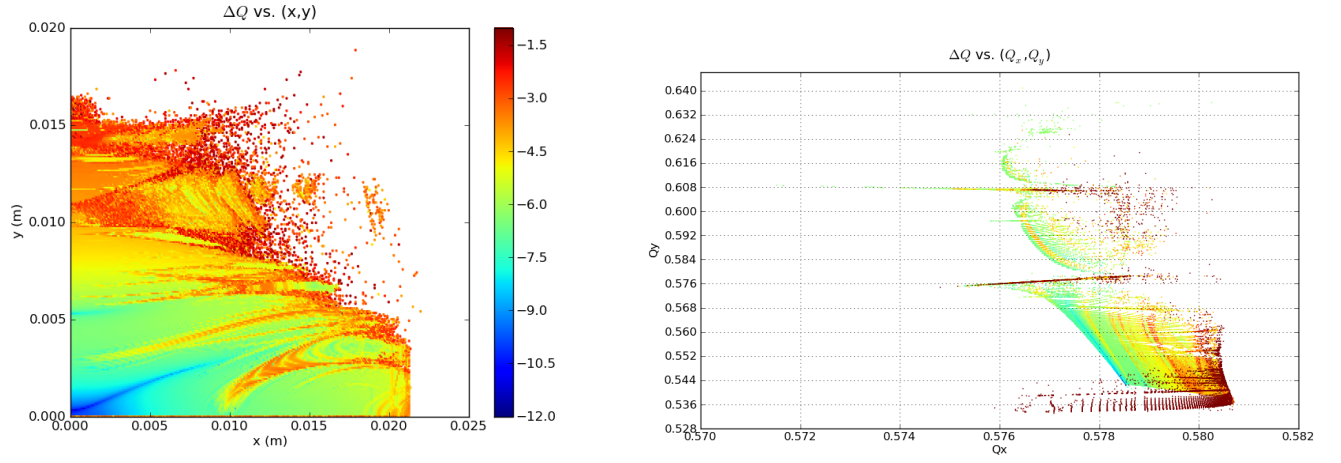


FIG. 8: FMA for optimized sextupole distribution, with new working point of  $(0.578, 0.542)$ . Horizontal and vertical grids are at the same spacing as in figure (5). The dynamic aperture for the original working point has a larger region of  $\delta Q < 10^{-6}$ , therefore the new working point has a smaller stable region in coordinate space. On the other hand, the torsion-positive side of the FM surface is significantly larger now, indicating a larger non-chaotic region in frequency space.